SERI/TP-257-3983
UC Category: 261
DE91002101

Spanwise Aerodynamic Loads on a Rotating Wind Turbine Blade

SERI/TP--257-3983

DE91 002101

C. P. Butterfield
D. A. Simms
W. P. Musial
G. N. Scott

October 1990

prepared for the
American Wind Energy Association
Windpower 90 Conference
Washington, D.C.
25-28 September 1990

Prepared under Task No. WE011001

Solar Energy Research Institute
A Division of Midwest Research Institute

1617 Cole Boulevard
Golden, Colorado 80401-3393

Prepared for the
U.S. Department of Energy
Contract No. DE-AC02-83CH10093

Spanwise Aerodynamic Loads on a Rotating Wind Turbine Blade

C.P. Butterfield
Dave Simms
Walt Musial
George Scott

Solar Energy Research Institute
1617 Cole Blvd.
Golden, Colorado, 80401
USA

Presented at the
American Wind Energy Association
Windpower 90 Conference
Washington, DC.
September 25-28, 1990

Abstract

Wind turbine performance and load predictions depend on accurate airfoil performance data. Wind tunnel test data are typically used which accurately describe two-dimensional airfoil performance characteristics. Usually these data are only available for a range of angles of attack from 0 to 15 deg, which excludes the stall characteristics. Airfoils on stall-controlled wind turbines operate in deep stall in medium to high winds. Therefore it is very important to know how the airfoil will perform in these high load conditions. Butterfield et al. [1] have shown that three-dimensional effects and rotation of the blade modify the two-dimensional performance of the airfoil. These effects are modified to different degrees throughout the blade span.

The Solar Energy Research Institute (SERI) has conducted a series of tests to measure the spanwise variation of airfoil performance characteristics on a rotating wind turbine blade. Maximum lift coefficients were measured to be 200% greater than wind tunnel results at the 30% span. Stall characteristics were generally modified throughout the span. Lift characteristics were unmodified for low to medium angles of attack. This paper discusses these test results for four spanwise locations.

Introduction

Wind turbine aerodynamic analyses depend on wind tunnel data to predict performance and loads. Stall-controlled wind turbines achieve peak power regulation through operation of airfoils in deep stall and therefore require airfoil performance data for high angles of attack (AOA). Turbine performance predictions using wind tunnel airfoil data typically underpredict the peak power and loads. Because good agreement was achieved at low wind speeds but not at high wind speeds, it was suspected that the airfoil inputs were at fault.

Dynamic loads have always been difficult to predict. Wright and Thresher [2] showed that dynamic analyses of wind tunnel tested rotors obtain reasonable agreement when the inflow was constant and wind shear was modeled accurately. This implies that the analyses are correct as long as stall is not present and all the inputs are correct. For the free-stream case, poor agreement was blamed on inaccurate airfoil input data and poor definition of the complex inflow. Poor modeling of unsteady aerodynamics may also be a contributor to inaccurate predictions. It was obvious that a better understanding was needed of airfoil performance on a rotating wind turbine blade.

Therefore the objectives of the program were to understand
(1) how airfoil performance is modified by rotation on a wind turbine blade
(2) what role dynamic stall plays in turbine performance and loads
(3) how turbulence affects aerodynamic performance, and finally
(4) how yawed operation of the turbine affects the rotor aerodynamics.

The approach that SERI followed was to first understand the basic flow state on the blade. Video cameras recorded flow patterns while pressure measurements were made at the 80% blade span during phase I as described by Butterfield [1] and at four spanwise locations during phase II. A vertical plane array of anemometers was used to measure the complex wind inflow. Strain gage measurements were made through the wind turbine to document the resulting loads.

Phase I testing focused on developing the instrumentation needed to perform these difficult tests and establish a correlation of 80% span wind turbine data with wind tunnel data. Butterfield and Nelson [3] describe these efforts and results from the comparisons.

Phase II tests were focused on understanding how these airfoil performance properties are modified throughout the blade span. This report will describe results from pressure distribution measurements made at four spanwise locations throughout the blade.

Test Description

A 10-m, three-bladed, downwind horizontal-axis wind turbine was used as a test platform. Molds were made to high tolerances so that airfoil coordinates would be accurately transferred to the test blades. The SERI S809 airfoil was used because extensive wind tunnel data were available for it. This airfoil is one of a family of airfoils designed specifically for

wind turbine use. Tangler [7] describes the airfoil as a 21% thick, laminar-flow airfoil with low roughness sensitivity.

Two blades were made with no instrumentation and a third was constructed with 124 pressure taps installed inside the blade. Butterfield et al. [4] describe the installation technique and the pressure measurement instrumentation for the first phase of this test program. Phase II testing required four chordwise pressure distributions located at 30%, 47%, 63%, and 80% blade spans. Pressure taps were located at 4% chord and 36% chord on the suction side of the airfoil for six additional spanwise locations. Figure 1 shows the wind turbine and basic statistics. Figure 2 shows the pressure tap spanwise locations on the blade and the tap chordwise locations on the airfoil for each of the four spanwise locations.

Four ESP-32 pressure transducers were installed inside the test blade near the chordwise distributed taps. Stainless steel tubes were fabricated into the blade skin to carry the surface pressures to each of the transducers. The tube lengths ranged from 4 cm to 7.4 cm and were 1 mm inside diameter. A microprocessor-based controller was used to electrically scan each of the transducers at a tap-to-tap frequency of 16,672 Hz. Thus each pressure channel was sampled at 521 Hz. Analog filters, set at 100 Hz, were used to prevent aliasing. Transfer functions were measured for each pressure channel to determine the electrical and acoustical dynamic characteristics. In all cases the dynamic response was flat in the region of interest.

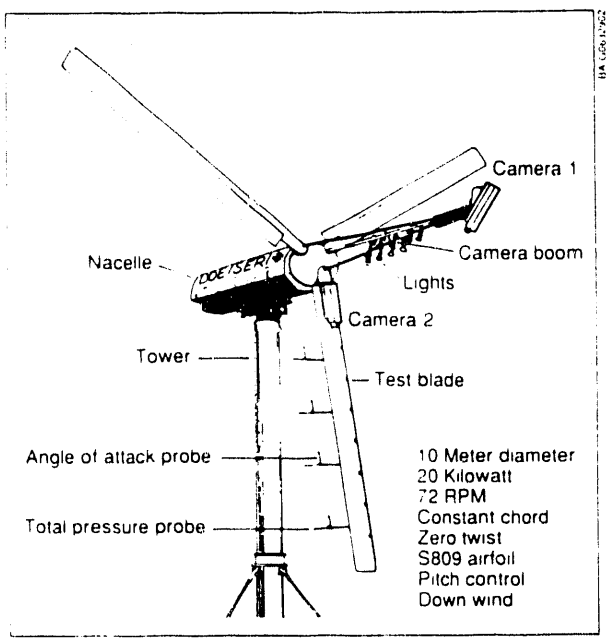

Figure 1. Test turbine description

The same pressure tap locations and instrumentation were used in wind tunnel tests at the Ohio State University (OSU) and Colorado State University (CSU) wind tunnels as described by Butterfield and Nelson [3] and Butterfield et al. [4]. By keeping the instrumentation, pressure tap location and airfoil identical between wind tunnel tests and rotating blade wind turbine tests, differences in the results would be more likely attributable to real differences in airfoil performance

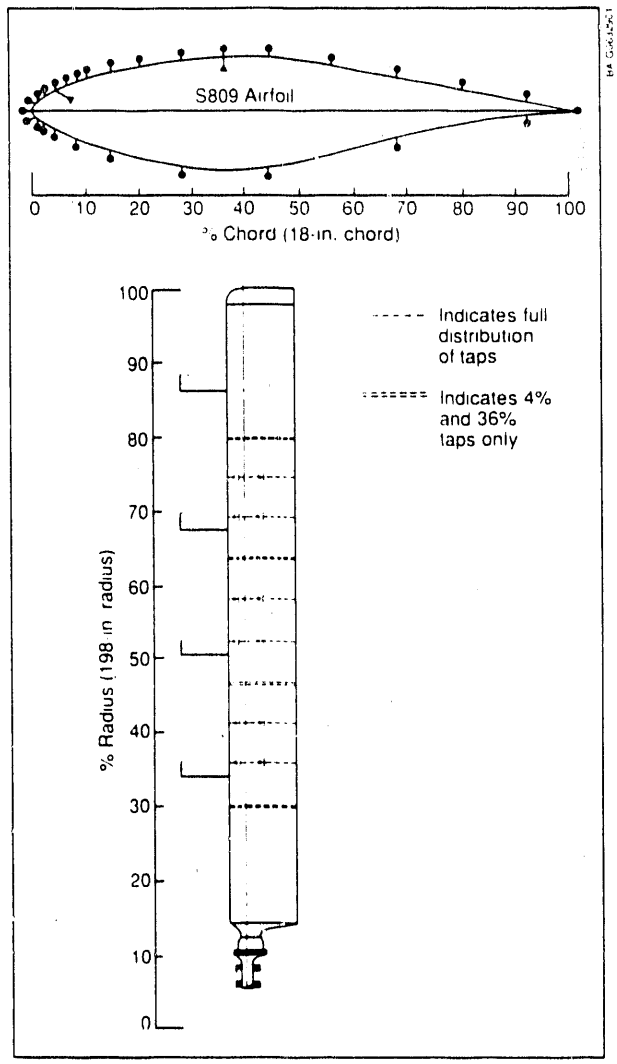

Figure 2. Blade layout

caused by three-dimensional and rotating-blade effects.

Dynamic pressure and local flow angle were measured at each of the four pressure distributions. Dynamic pressure was measured using a total pressure probe with an internal angle of 45 deg. This probe was tested in the CSU wind tunnel and found to give accurate total pressure measurements for angular misalignments up to 40 deg. The flow angle probe was also tested in the wind tunnel while mounted on the airfoil. Upwash due to circulation effects causes local flow angles to deviate from the geometric angle of attack. In this test the deviations were measured and used to correct the rotating-blade measured angles. Butterfield [5] describes these corrections as well as dynamic response tests performed on the probe.

Data Processing

After the raw data were recorded, calibration coefficients were applied. Pressure instrumentation calibrations were recorded every five minutes of testing. This enabled calibration coefficients to be updated frequently enough to reduce the thermal drift errors to less than 3% of the local dynamic pressure. The procedure was laborious but assured accurate

engineering data for later processing.

The reference pressures for each transducer located in the blade were transferred from the hub to the transducer through a tube. The effects of centrifugal force on air in the tube were corrected per equation (1), which is very similar to the procedure described by Hurst and Owen [6] in equation (2). Hurst's equation assumed that the transducer was located at the axis of rotation and that a long tube was run from the transducer down the blade to the surface pressure tap. Equation (2) includes compressibility effects which are negligible and not included in equation (1).

In this test program two centrifugal force corrections were needed. The first corrected the reference tube pressures from the axis of rotation to the transducer, and the second corrected the pressures in the tubes leading from the transducer to the blade surface.

$$P_{ref} = P_{atm} + \frac{1}{2}\rho(r\omega)^2 \tag{1}$$

$$P_{surface} = P_{meas}^{\frac{\omega^2 r^2}{2RT}} \tag{2}$$

where

P_{ref} = reference pressure at transducer
P_{atm} = atmospheric pressure
$P_{surface}$ = actual surface pressure
P_{meas} = measured surface pressure
ω = rotor speed
K = gas constant
T = temperature
r = radius to reference port or surface pressure tap
ρ = air density

To obtain normalized pressure coefficients (C_p), dimensional pressure data were divided by local dynamic pressure per equation (3). Dynamic pressure was established in two ways. First, atmospheric pressure was subtracted from measured total pressure to get a local, measured dynamic pressure (Q_{meas}) using equation (4). The second method derived the local value of dynamic pressure (Q_{der}) by using equation (5) plus the disk-averaged wind speed (measured from the vertical plane array), the rotor angular speed, and the radius to the pressure tap.

$$C_p = \frac{P_{surface} - P_{atm}}{Q_{meas}} \tag{3}$$

$$Q_{meas} = P_{tot} - P_{atm} \tag{4}$$

$$Q_{der} = \frac{1}{2}\rho(V^2 + (r\omega)^2) \tag{5}$$

where

Q_{meas} = measured dynamic pressure
Q_{der} = derived dynamic pressure
V = disk-averaged wind speed
C_p = normalized pressure coefficient
P_{tot} = measured total pressure.

Both methods gave similar results that agreed with wind tunnel data at low AOAs. At high AOAs (greater than 25 deg) on the 30% blade span pressure distribution, the measured Q_{meas} method gave values of pressure coefficient (C_p) greater than one at the stagnation point. This indicates that actual value of Q was lower than the leading-edge stagnation pressure. The stagnation pressure should always be the same value as the dynamic pressure. Because of this problem all the pressure data presented in this report were normalized by the calculated dynamic pressure (Q_{der}).

All the pressure data were digitized at a 520-Hz sample rate. Data were later pre-averaged by a factor of 52 to obtain a final 10-Hz sample rate. These data were then sorted into bins using the measured angle of attack as the independent variable. Analog filters were used to eliminate aliasing of the data. These filters were four-pole Butterworth type, set at a 100-Hz roll-off frequency.

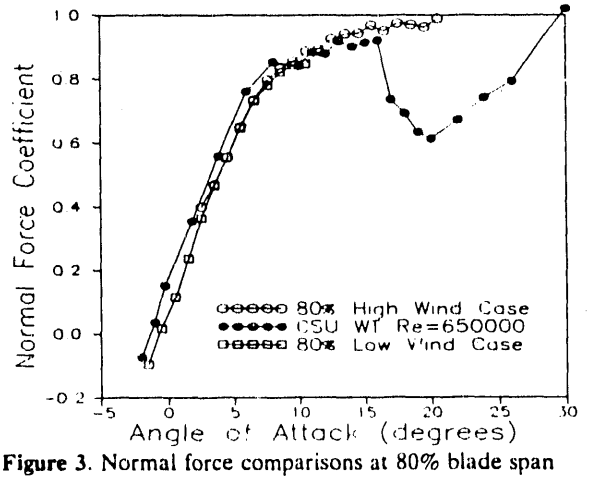

Figure 3. Normal force comparisons at 80% blade span

Results

Figure 3 shows normal force coefficients (C_n) for both the CSU wind tunnel (WT) and the 80% blade span on the wind turbine. The correlation is good for angles below 15 degrees. Beyond 15 degrees, stall causes normal force coefficients to fall abruptly for the wind tunnel data while the rotating blade (RB) data drop very gradually with increasing AOA. This is consistent with results from phase I testing as described by Butterfield et al. [1]. Figure 4 shows how the airfoil performs at the 30%, 47%, 63%, and 80% blade span locations by comparison. All curves agree at low AOA while the two mid-span stations (47% and 63%) show an increase of 10% in $C_{N_{max}}$ and a leveling of values for higher AOAs. The 80% station $C_{N_{max}}$ did not increase above that of the wind tunnel but did experience the same leveling off at higher angles of attack.

At the 30% span the results are very different. The magnitude of C_N continues to increase with increasing AOA. A maximum

value of 2.0 was recorded at an AOA of 30 deg, which is more than 200% greater than the maximum value measured in the wind tunnel. Lift coefficients show similar characteristics as shown in Figure 5.

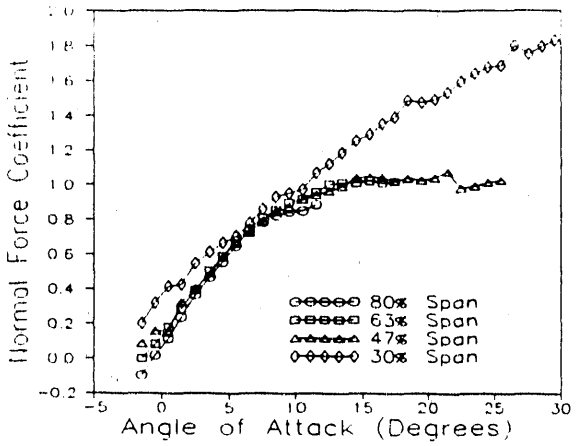

Figure 4. Normal force comparisons throughout blade span

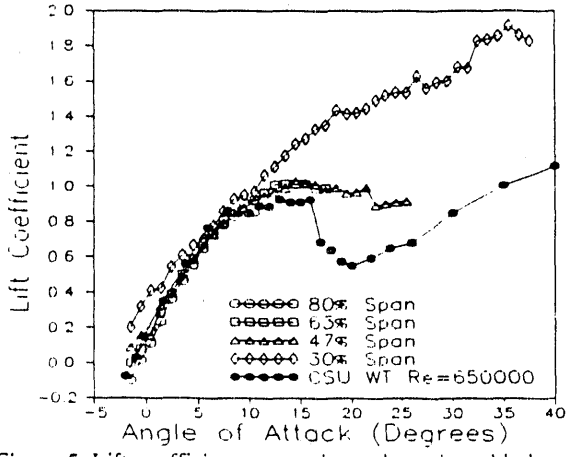

Figure 5. Lift coefficient comparisons throughout blade span

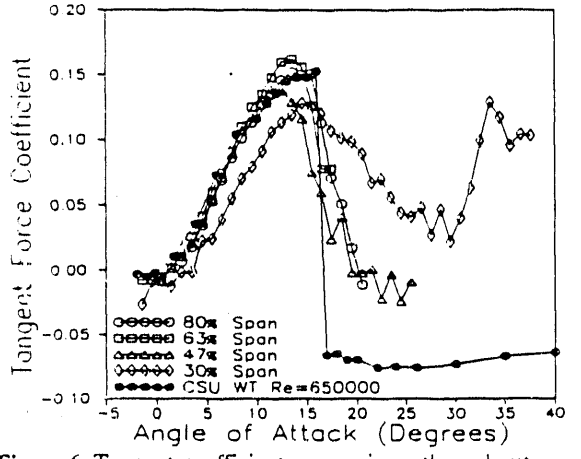

Figure 6. Tangent coefficient comparisons throughout blade span

Tangent force coefficients were compared in Figure 6. Wind tunnel data again show good agreement with RB data for low AOA. The wind tunnel data show a very sharp drop at stall. The RB data show a very gradual drop-off after stall. This discrepancy can have a large effect on rotor torque because the blade pitch angle and hence the tangent forces are closely aligned with the plane of rotation.

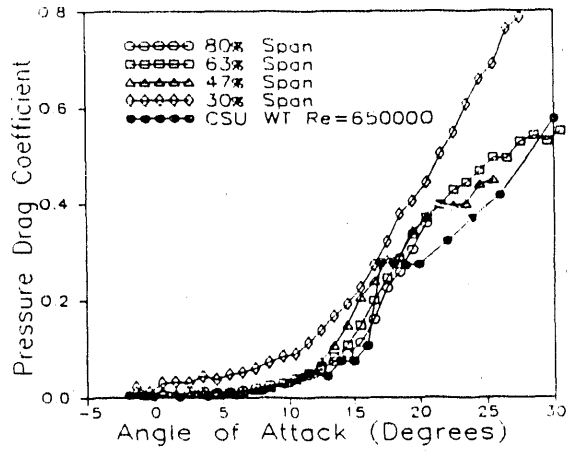

Figure 7. Pressure drag coefficient comparisons throughout blade span

Pressure drag data are shown in Figure 7. Below stall the wind turbine blade data agree well with the wind tunnel data, as was typical in previous comparisons. Beyond stall the wind turbine data are greater than wind tunnel values. This is a surprising result considering that the tangent forces were greater than wind tunnel data. However equation (5) shows that C_n can dominate the drag term for nominal angles of 20 deg and large values of C_n.

$$C_{dp} = C_N \sin(AOA) - C_t \cos(AOA) \quad . \qquad (6)$$

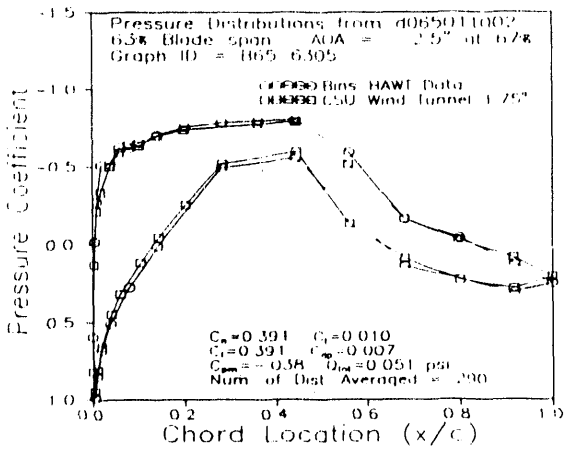

Figure 8. Pressure distributions at 63% blade span

Pressure distributions were compared for all the AOAs measured. Figure 8 shows one such comparison at 63% span and a low AOA of 2.5 deg. The good correlation at this low angle helps to reinforce the integrity of the data-acquisition system and data-reduction techniques. It also indicates that the airfoil is behaving in a two-dimensional way as long as the flow is attached.

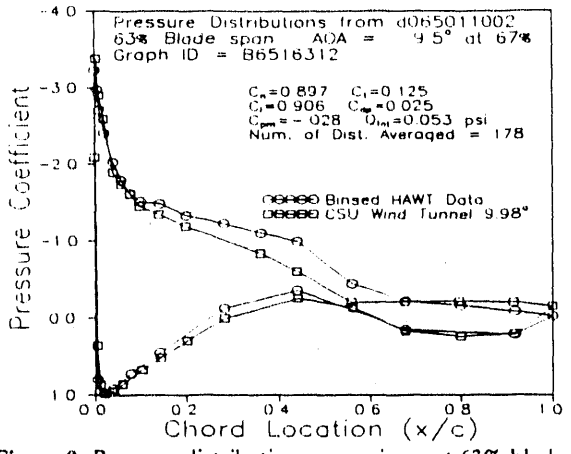

Figure 9. Pressure distribution comparisons at 63% blade span

Figure 9 shows the same 63% span station at 9.5 deg AOA. Here there is good correlation between suction peaks as well as the high pressure (bottom) side pressure coefficients. Separation is evident from the flat region on the afterbody of the low pressure side of the airfoil. The pressure drop at 55% to 65% chord indicates flow attachment. The wind turbine data show the attachment point at 65% chord while the wind tunnel data show attachment at 55% chord. This is a consistent discrepancy between the two data sets. As the AOA rises and stall separation progresses forward from the trailing edge, the point of separation is delayed for the wind turbine data. The difference in integrated area under the pressure distribution curves is 5% to 10%, depending on the AOA.

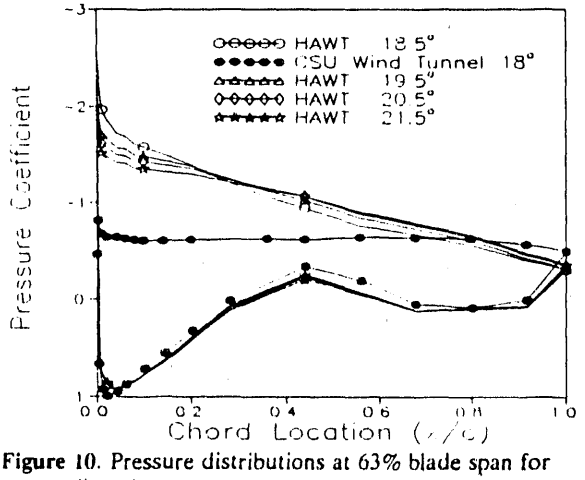

Figure 10. Pressure distributions at 63% blade span for post-stall angles

Figure 10 shows a wind tunnel pressure distribution at 18.5 deg AOA and a family of wind turbine curves for the 63% span ranging from 18.5 deg to 21.5 deg AOA. The wind tunnel data show a flat distribution on the low pressure side of the airfoil, implying leading edge separation. The wind turbine data clearly show suction peaks and pressure gradients, a condition that persists to AOAs higher than 23.5 deg. Figure 11 shows data for similar conditions at the 80% span. The suction peak appears to be more pronounced at this station

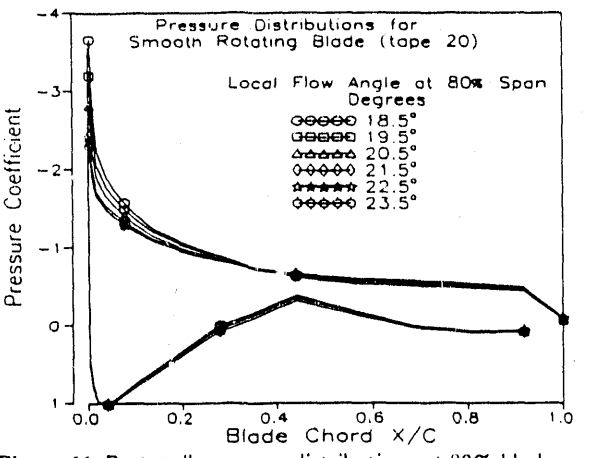

Figure 11. Post-stall pressure distributions at 80% blade span

and the pressure gradient following the peak is pronounced. In both cases the existence of a suction peak and more negative pressures along the low pressure side of the airfoil result in higher than expected normal force coefficients, which were shown in Figure 4. Results from the 47% span pressure measurements are very similar to those shown for the 63% span and are not shown in this report.

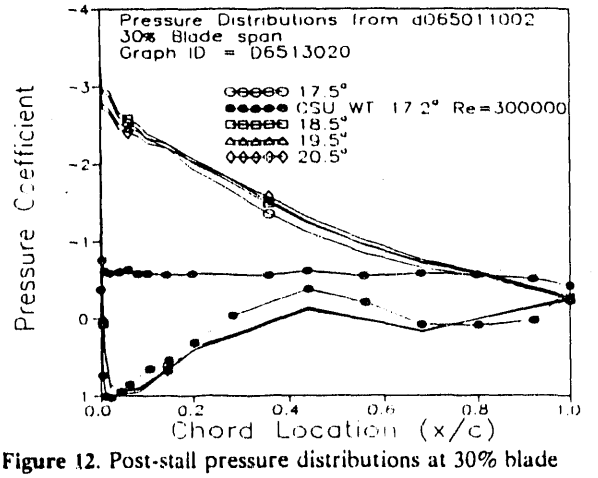

Figure 12. Post-stall pressure distributions at 30% blade span

Figure 12 shows results from the 30% span measurements. At this inboard location the same trend is continued; there is good correlation at low angles (not shown) and delayed stall at high angles. In this case the pressure coefficients are more negative on the downwind side of the airfoil than at the outboard stations. Integration of the larger area under the rotating-blade curve results in higher values of C_n and C_l at high AOAs.

This explains why the integrated values are higher, but it does not explain why the pressure distributions are consistently different than wind tunnel data measured on the same airfoil. Usually pressure gradients such as those shown in Figure 12 are associated with attached flow. These pressure gradients actually exist even though the flow is separated over most of the airfoil surface. This was demonstrated using video data of tufts time correlated with pressure distributions. The results of this analysis are shown by Scott et al. [8]. The answers to these questions are not known. Spanwise flow, in the separation region, may be

causing the pressure gradients or possibly vorticity in the separation bubble. Future tests and data analysis will be focused on the answers to these questions.

Conclusions

The data presented demonstrate that airfoils behave as they would in the wind tunnel for low to moderate angles of attack. Near stall the wind turbine airfoils show a delay in stall due to a combination of suction peak persistence and high negative pressures on the suction side of the airfoil. This results in high normal forces and high tangent forces in the post-stall region. Because of this modified airfoil behavior, wind tunnel stall data may not be accurate for stall control wind turbine design purposes. However, it is not clear what causes this behavior or what effect blade planform (twist and taper) will have on the airfoil performance.

Future Work

The dynamic behavior of the stalling process is very important to wind turbine design. The effects of blade twist and taper could also play an important role in the airfoil performance. Many questions still exist about what causes modification of airfoil performance. These issues will be addressed in future data analysis and ongoing tests at SERI.

Acknowledgements

The authors wish to acknowledge the Department of Energy for the support of this work through contract number DE-AC02-83CH10093. Other contributors include Al Eggers, Craig Hansen, Bob Akins, Bob Thresher, Mike Jenks, and Diane Pipan-Logan.

References

1. Butterfield, C. P., Scott, G., and Musial, W., "Comparison of Wind Tunnel Airfoil Performance Data with Wind Turbine Blade Data," SERI/TP-257-3799, Golden, CO. Solar Energy Research Institute (July 1990).

2. Wright, A. D., and Thresher, R. W., "A Comparison of Predicted Wind Turbine Blade Loads to Test Measurements," SERI/TP-217-3070, Golden, CO. Solar Energy Research Institute (January 1987).

3. Butterfield, C. P., and Nelson, E., "Aerodynamic Testing of a Rotating Wind Turbine Blade," SERI/TP-257-3490, Golden, CO. Solar Energy Research Institute (January 1990).

4. Tangler, J., and Somers, D., "Status of the Special-Purpose Airfoil Families," SERI/TP-217-3264, Golden, CO. Solar Energy Research Institute (December 1987).

5. Butterfield, C. P., Jenks, M., Simms, D., and Musial, W., "Aerodynamic Pressure Measurements on a Rotating Wind Turbine Blade," SERI/TP-257-3695, Golden, CO. Solar Energy Research Institute (May 1990).

6. Butterfield, C. P., "Three-Dimensional Airfoil Performance Measurements on a Rotating Wing," SERI/TP-217-3505, Golden, CO. Solar Energy Research Institute (June 1989).

7. Hurst, D. W., and Owen, D. T., "Nacelle Installation Effects on Propeller Blade Surface Pressure Distributions," University of Southampton, England, 0096-736X/88/9606-0940, 1988 Society of Automotive Engineers, Inc.

8. Scott, G., Butterfield, C. P., Simms, D., and Musial, W., "Correlations of Flow Visualization and Pressure Distribution Data on a Wind Turbine Blade," 14th ASME-ETCE Conference Proceedings, January 1991, Houston, TX.

END

DATE FILMED

11/16/90